Structure of Ala24/Asp61 → Asp24/Asn61 Substituted Subunit *c* of *Escherichia coli* ATP Synthase: Implications for the Mechanism of Proton Transport and Rotary Movement in the F_o Complex[†]

Oleg Y. Dmitriev,[‡] Frits Abildgaard,[§] John L. Markley,[§] and Robert H. Fillingame*,[‡]

Department of Biomolecular Chemistry, University of Wisconsin Medical School, and Department of Biochemistry, University of Wisconsin, Madison, Wisconsin 53706

Received December 27, 2001; Revised Manuscript Received February 21, 2002

ABSTRACT: The structure of the A24D/D61N substituted subunit *c* of *Escherichia coli* ATP synthase, in which the essential carboxylate has been switched from residue 61 of the second transmembrane helix (TMH) to residue 24 of the first TMH, has been determined by heteronuclear multidimensional NMR in a monophasic chloroform/methanol/water (4:4:1) solvent mixture. As in the case of the wild-type protein, A24D/D61N substituted subunit *c* forms a hairpin of two extended α-helices (residues 5−39 and 46−78), with residues 40−45 forming a connecting loop at the center of the protein. The structure was determined at pH 5, where Asp24 is fully protonated. The relative orientation of the two extended helices in the A24D/D61N structure is different from that in the protonated form of the wild-type protein, also determined at pH 5. The C-terminal helix is rotated by 150° relative to the wild-type structure, and the N-terminal helix is rotated such that the essential Asp24 carboxyl group packs on the same side of the molecule as Asp61 in the wild-type protein. The changes in helix−helix orientation lead to a structure that is quite similar to that of the deprotonated form of wild-type subunit *c*, determined at pH 8. When a decameric ring of *c* subunits was modeled from the new structure, the Asp24 carboxyl group was found to pack in a cavity at the interface between two subunits that is similar to the cavity in which Asp61 of the wild-type protein is predicted to pack. The interacting faces of the packed subunits in this model are also similar to those in the wild-type model. The results provide further evidence that subunit *c* is likely to fold in at least two conformational states differing most notably in the orientation of the C-terminal helix. Based upon the structure, a mechanistic model is discussed that indicates how the wild-type and A24D/D61N subunits could utilize similar helical movements during H^+ transport-coupled rotation of the decameric *c* ring.

H^+-transporting F_1F_o ATP synthases utilize the energy of an H^+ electrochemical gradient to drive formation of ATP from ADP and P_i. Closely related enzymes are found in the plasma membrane of eubacteria, the inner membrane of mitochondria, and the thylakoid membrane of chloroplasts (*1*). The enzymes are composed of distinct extramembranous and transmembranous sectors, termed F_1 and F_o, respectively. Proton movement through F_o is reversibly coupled to ATP synthesis or hydrolysis in catalytic sites on F_1. Each sector of the enzyme is composed of multiple subunits with the simplest composition being $\alpha_3\beta_3\gamma\delta\epsilon$ for F_1 and $a_1b_2c_{10}$ for F_o in the case of the *Escherichia coli* enzyme (*2*−*4*). Homologous subunits are found in mitochondria and chloroplasts. An atomic resolution X-ray structure of the $\alpha_3\beta_3\gamma$ portion of bovine F_1 shows the three α and three β subunits alternating around a centrally located γ subunit, wherein the γ subunit interacts asymmetrically with the three $\alpha\beta$ subunit pairs (*5*). Subunit γ was subsequently shown to rotate within the $\alpha_3\beta_3$ hexamer during catalysis (*6*−*8*). Rotation of subunit γ is thought to change the binding affinities in catalytic sites and alternately promote tight substrate binding and then product release during catalysis (*9*). The γ and ϵ subunits interact with each other and are known to rotate as a fixed unit (*10*, *11*). The X-ray structures of $\gamma\epsilon$ and $\alpha_3\beta_3\gamma\epsilon$ were reported recently (*12*, *13*). During ATP synthesis, the rotation of $\gamma\epsilon$ must be driven by proton flux through F_o. Recent evidence now supports a rotary mechanism for ATP synthesis in which proton transport-coupled rotation of an oligomeric ring of 10 *c* subunits in the membrane is coupled to rotary movement of subunits $\gamma\epsilon$ between the alternating catalytic sites (*14*−*17*). In this model, the sequential protonation and deprotonation of Asp61 at the center of the second transmembrane helix (TMH)[1] of subunit *c* is coupled with a stepwise movement of the rotor, i.e., by 36° (*18*−*20*). Although a detailed structure of the

[†] Support for this study was provided by U.S. Public Health Service Grant GM-23105. The NMR experiments were carried out at the National Magnetic Resonance Facility at Madison with support from the NIH Biomedical Technology Program (RR02301) and additional equipment funding from the University of Wisconsin, the NSF Academic Infrastructure Program (BIR-9214394), the NIH Shared Instrumentation Program (RR02781 and RR08438), the NSF Biological Instrumentation Program (DMB-8415048), and the U.S. Department of Agriculture.

* To whom correspondence should be addressed: Department of Biomolecular Chemistry, 1300 University Ave., University of Wisconsin Medical School, Madison, WI 53706-1532. Telephone: (608) 262-1439. Fax: (608) 262-5253. E-mail: rhfillin@facstaff.wisc.edu.

[‡] University of Wisconsin Medical School.

[§] University of Wisconsin.

10.1021/bi012198l CCC: $22.00
Published on Web 03/29/2002

complete F_o complex is not at hand, the current structural and biochemical evidence summarized below fits well with the rotary hypothesis.

Several experimental approaches have contributed to our present understanding of the structural arrangement of subunit *c* in F_o. The structure of monomeric subunit *c* was determined by NMR in a membrane-mimetic solvent, i.e., a monophasic chloroform/methanol/H_2O mixture (4:4:1), initially at pH 5 where Asp61 is protonated (*21*). The protein was found to fold as a hairpin of two α-helices, packed in parallel and connected by a short polar loop, with the helix−helix interactions in accord with those expected for the protein in the native membrane. The carboxyl side chain of Asp61 was packed at the center of the "front" flattened face of the interacting helices. On the basis of the NMR model and approximately 20 distance constraints derived by intersubunit Cys−Cys cross-linking (*22*, *23*), a model for an oligomeric ring of *c* subunits in the membrane was calculated (*24*). In the model, the multiple copies of subunit *c* were proposed to be arranged in a cylinder-like structure such that the TMHs form two concentric rings with the N- and C-terminal helices positioned in the inner and outer circle of the ring, respectively. Residues within the polar loops at the top of the cylinder were known to interact with the γ and ϵ subunits of F_1 in the native enzyme (*25*, *26*), and this interaction was modeled initially on the basis of the NMR structures of subunits ϵ and *c* (*27*, *28*) and now the X-ray structure of $\gamma\epsilon$ (*12*). The model for the oligomeric ring of subunit *c* in F_o is supported by electron and atomic force microscopy and more recently by direct crystallographic observations (*29*−*34*). The number of *c* subunits in the complex is at present the subject of controversy, with numbers in the range of 10−14 being proposed for different species (*4*, *32*−*34*). We initially favored the number 12, based upon the expression and cross-linking of active, genetically fused dimers and trimers of subunit *c* (*23*). However, we now believe that the preferred number of *c* subunits in the oligomeric ring of *E. coli* is 10, based upon coexpression and cross-linking of genetically fused trimers and tetramers into decameric structures (*4*).

Subunits *a* and *b* are located outside the *c* ring perimeter (*29*−*31*), subunit *a* being in contact with TMH-2 of subunit *c* (*35*). Subunit *b* is present in two copies and probably serves as the stalk of the stator holding the $\alpha_3\beta_3$ subunits of F_1 in a fixed position relative to the transmembrane regions of subunits *a* and *b* (*36*−*38*). A structure of the single, membrane-anchoring TMH of subunit *b* (residues 1−34) was determined by NMR using a chloroform/methanol/H_2O mixture (4:4:1) as the solvent (*39*). This helix can be cross-linked to *c*TMH-2 and lends support to the idea that subunit *b* packs outside the *c* ring (*40*). Direct evidence that subunit *b* forms a peripheral stalklike structure extending to the top of the F_1 molecule was provided by electron microscopy and cross-linking (*36*−*38*, *41*, *42*). Subunit *a* folds in the membrane with five TMHs (*43*, *44*). Residues in *a*TMH-4 have been implicated in the proton transport mechanism and may provide portions of the access channels from *c*Asp61 to the two sides of the membrane. Residue *a*R210 in *a*TMH-4 is proposed to facilitate proton release by lowering the pK_a of Asp61 as it passes the *a* subunit of the stator (*20*, *45*). Following introduction of appropriate Cys residues, *a*TMH-4 and *c*TMH-2 can be cross-linked over a membrane-spanning length of 19 residues in each helix (*35*). Oddly, the face of *c*TMH-2 that cross-links to *a*TMH-4 packs next to *c*TMH-1 in the NMR structure and *c* ring model (*21*, *24*), rather than on the outer surface. Further, in the oligomeric ring model, *c*Asp61 is packed between subunits where it would be inaccessible to interaction with *a*R210 (*24*). In a more recently determined NMR structure of subunit *c* (*46*), determined at pH 8 under conditions where Asp61 should be ionized (*47*), *c*TMH-2 is rotated by 140° relative to the pH 5 structure. The cross-linking results and new NMR structure have led to the suggestion that *c*TMH-2 may rotate during the proton translocation cycle, which would make *c*Asp61 accessible to *a*Arg210 with the helical rotation in turn driving the stepwise movements of the *c* ring (*35*, *46*, *48*).

The essential aspartyl residue of subunit *c* can be moved from position 61 in TMH-2 to position 24 in TMH-1 with retention of significant function, as originally shown by Miller et al. (*49*) with the D24G61 double mutant (Ala24/Asp61 → Asp24/Gly61).[2] Subsequently, considerably greater function was shown with the D24N61 substituted protein (*50*). Other aspartate-interchange mutants, with third site-optimizing mutations in subunit *a*, grow and function as well as the wild type (*51*). Given the suggestion that *c*Asp61 of the wild-type protein should gain access to *a*Arg210 by a swiveling of *c*TMH-2 (*46*, *48*), how could the D24G61 or D24N61 proteins possibly function, or is the suggested mechanism not valid? To gain insight into this question, we have determined the NMR structure of D24N61 subunit *c* at pH 5 where Asp24 was shown to be protonated [pK_a = 6.9 (*47*)]. The structure closely resembles the structure of wild-type subunit *c* at pH 8, where Asp61 is deprotonated and *c*TMH-2 rotated relative to the structure at pH 5. The results suggest that the essential aspartate, whether at position 61 or position 24, may gain accessibility to *a*R210 by a swiveling of helices within a single *c* subunit to shift the position of the carboxyl in concert with rotation of *c*TMH-2.

EXPERIMENTAL PROCEDURES

Sample Preparation for NMR. D24N61 subunit *c* was prepared from *E. coli* strain JH618, which contains copies of the mutant subunit *c* gene on the chromosome and on a pBR322-derived plasmid. Strain JH618 is genetically equivalent to strain MEG119 which is used for the purification of the wild-type protein (*52*). Uniform labeling with ^{15}N and ^{13}C was achieved by growing cells on a minimal medium containing 15 mM $^{15}NH_4Cl$ and 0.2% [^{13}C]glucose as sources of nitrogen and carbon, respectively. Subunit *c* was purified as described previously (*52*). Samples for NMR contained 0.6 mL of 2.0 mM subunit *c* in a $CDCl_3/CD_3OH/H_2O$ mixture (4:4:1) containing 50 mM NaCl. The pH of the sample was adjusted to 5.0 without correction for the isotope effect at the glass electrode.

[1] Abbreviations: DCCD, dicyclohexylcarbodiimide; NMR, nuclear magnetic resonance; HSQC, heteronuclear single-quantum coherence; NOE, nuclear Overhauser enhancement; NOESY, NOE spectroscopy; rmsd, root-mean-square deviation; TMH, transmembrane helix.

[2] We henceforth identify double mutants by referring to the residues at the final position only, i.e., A24D/D61N being D24N61 subunit *c*.

Table 1: Summary of Constraints and Statistics for the D24N61 Subunit *c* Structure Calculation

no. of NOE-derived distance constraints (total of 1307)	
intraresidue	284
sequential	366
medium-range ($1 < \|i - j\| \leq 4$)	604
long-range ($\|i - j\| \geq 4$)	53
hydrogen bond constraints	48
mean global pairwise backbone rmsd (Å)	0.63 ± 0.15
mean global pairwise heavy atom rmsd (Å)	0.97 ± 0.14
consistent distance constraint violations above 0.2 Å	0

NMR Spectroscopy and Structure Calculation. NMR data were collected on a Bruker DMX500 spectrometer with triple-axis pulsed field gradient capability at 300 K. Pulsed field gradients were used for coherence selection and sensitivity enhancement. Backbone assignments were obtained from HSQC (*53*), HNCO (*54*), HNCA (*55*), CBCA(CO)NH (*56*), HCACO (*57*), HN(CO)CACB (*58*), and HN(CO)CA (*58*) spectra. Side chains were assigned using HCCH-COSY (*59*), HCCH-TOCSY (*59*), HC(CO)NH (*60*), and TOCSY-HSQC (*61*) experiments. Exchange rates for amide protons were measured by diluting a sample in a $CDCl_3/CD_3OH/H_2O$ mixture with 2 volumes of fully deuterated solvent and then recording a series of HSQC spectra at intervals between 1 and 36 h. Distance constraints were obtained from three-dimensional (3D) ^{15}N- or ^{13}C-separated NOESY (*61*, *62*), 3D NOE-HNCO (*63*), or four-dimensional (4D) $^{13}C,^{15}N$- or $^{13}C,^{13}C$-separated NOESY (*64*, *65*) spectra. Spectral data were processed using Felix 95.0 software (Accelrys, Inc., San Diego, CA). The program ChiFit (*66*) was used to pick peaks.

The structure was calculated from 1307 distance constraints and 48 hydrogen bond constants (see Table 1). Two hundred initial structures were calculated using simulated annealing as implemented in DYANA (*67*). The 10 lowest-energy structures were additionally minimized using the AMBER force field as implemented in "Discover" (Accelrys, Inc.). The quality of the structures was checked using PROCHECK (*68*). The coordinates were deposited with the Protein Data Bank as entry 1L6T. NMR data were deposited at BioMagResBank as entry 5326. Molecular modeling was carried out using MOLMOL (*69*) and CNS (*70*).

Modeling the D24N61 Subunit c Oligomer. A model of the D24N61 subunit *c* oligomer was built on the basis of the wild-type subunit *c* ring model (*24*). The wild-type model was calculated by molecular dynamics and energy minimization beginning with the monomeric structure at pH 5 using 21 intersubunit distance constraints derived from Cys−Cys cross-linking of subunits in the intact enzyme. The most recent experimental data indicate that the number of *c* subunits in the F_o complex of *E. coli* (*4*) and mitochondria (*32*) is likely to be 10 rather than 12, and the rings were therefore constructed with 10 subunits. The D24N61 subunit *c* monomers were aligned with the wild-type ring structure by minimizing the backbone rmsd between the helical segments of residues 4−39 and 46−77 in the respective structures. The structure was energy minimized by applying noncrystallographic symmetry constraints and harmonic restraints to the positions of the Cα atoms. The quality of the resulting structure was analyzed by PROCHECK (*68*) and found to meet normal standards.

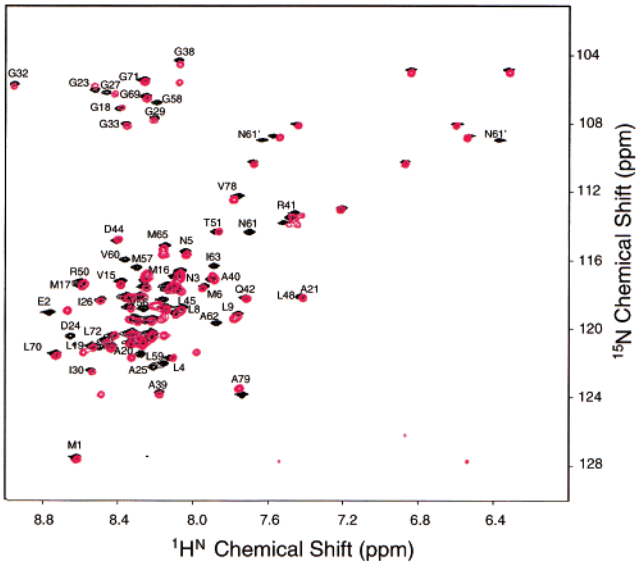

FIGURE 1: Overlay of $^1H,^{15}N$ HSQC spectra of the D24N61 (black) and wild-type (red) subunit *c* proteins. Assignments of backbone amide resonances are shown in uncrowded regions of the spectrum. The signals of Asn61 side chain resonances are also indicated.

RESULTS

Structure Determination. The structure determined was of D24N61 subunit *c* dissolved in the chloroform/methanol/water mixture, the solvent that was previously used in obtaining the structures of wild-type subunit *c* (*21*), the A20P/P64A substituted subunit *c* (*71*), and the N-terminal fragment of subunit *b* (*39*). To make the structural comparison meaningful, the spectra were recorded under conditions identical to those used for the wild-type protein (*21*). Almost all the backbone chemical shifts in the mutant protein were readily assigned. Combination of HCCH-COSY and HCCH-TOCSY data with data from $[^{15}N,^1H]$TOCSY-HSQC and H(CCO)NH experiments allowed assignment of most of the side chain chemical shifts as well.

An overlay of the two-dimensional $^{15}N,^1H$ chemical shift correlation spectra of the wild-type and D24N61 proteins is shown in Figure 1. The fingerprints of the two proteins are quite similar. Significant differences in amide chemical shifts are seen in residues around the sites of substitution at positions 24 and 61 (Figure 2C). In helix 1, the chemical shifts of A20, I22, A25, and I28 deviate the most from those of the wild type. In helix 2, residues 55−62 exhibit large deviations.

As noted before (*21*, *71*), the high degree of chemical shift degeneracy and spectral overlap in signals from the many aliphatic side chains cause numerous ambiguities in NOE assignment. The use of 4D NOESY experiments and the combination of 3D $[^{15}N,^1H]$NOESY-HSQC and NOE-HNCO experiments were very helpful in resolving these ambiguities. As an example, the 4D $[^{13}C,^{15}N]$NOESY allowed resolution of 110 medium-range $H\alpha_i-HN_{i,i+3}$ and $H\alpha_i-HN_{i,i+4}$ NOEs typical for largely α-helical subunit *c* (Figure 3). Despite its relatively low resolution and sensitivity, 4D $^{13}C,^{13}C$-separated NOESY was a useful complement to 3D ^{13}C-separated NOESY in the assignment of side chain NOEs. Summaries of the NOE information used for determining the structure of D24N61 subunit *c* are shown in Figure 2 and Table 1.

The final family of 10 structures had rmsds of 0.63 ± 0.15 Å for the backbone atoms and 0.97 ± 0.14 Å for all

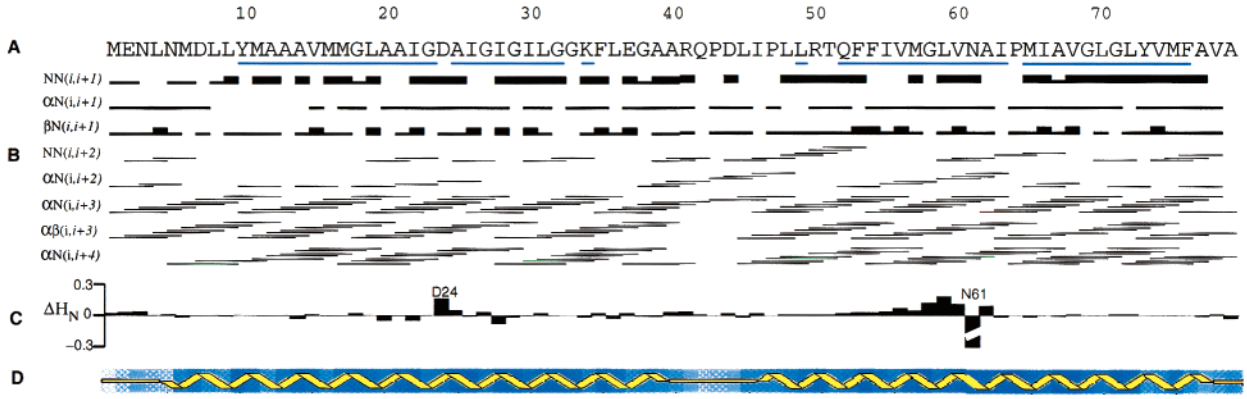

FIGURE 2: Summary of NMR data for D24N61 substituted subunit *c*. (A) Amino acid sequence showing residues with slowly exchanging amide protons underlined. (B) Sequential and medium-range NOEs. (C) The difference in chemical shift for amide protons for mutant minus wild-type subunit *c*. (D) Secondary structure elements and predicted solvent accessibility (lighter shading corresponds to higher accessibility) as determined by PROCHECK (*67*) for the final structure.

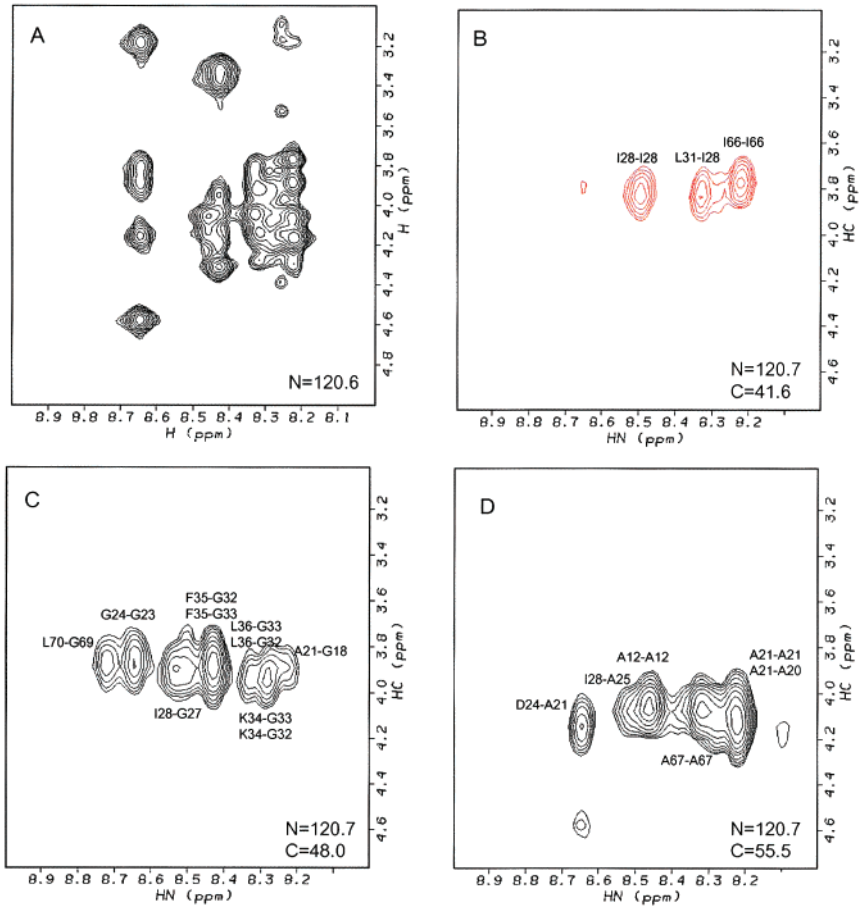

FIGURE 3: Example of resolving signal overlap in the NOESY spectra of subunit *c* by 4D $^{13}C,^{15}N$-separated NOESY. (A) A plane from the 3D ^{15}N-separated NOESY spectrum. (B−D) Three slices from corresponding series of planes from 4D $^{13}C,^{15}N$-separated NOESY spectra. NOE assignments are shown in panels B−D. Peaks in panel B are folded into the spectrum with opposite sign.

heavy atoms of residues 3−77. The conformation of the protein backbone in the polar loop region (residues 40−45) is particularly well defined with an rmsd of 0.19 ± 0.07 Å. No consistent distance constraint violations exceeded 0.3 Å (Table 1). In the 10 best structures, 88.6% of the residues were found in the most favored regions of the Ramachandran plot, with 11.1% in the additionally allowed, 0.3% in the generously allowed, and no residues in disallowed regions.

Structure of D24N61 Subunit c. As with the wild-type protein, the structure of D24N61 subunit *c* is best described as a hairpin of two α-helices extending from residues 5−39 and 46−78 connected by a short loop (Figure 2D). The packing of the two helices in the structure (Figure 4A) is determined by long-range distance constraints derived from 49 long-range NOEs. The interhelical NOEs do differ slightly from those seen in the wild-type protein at pH 5 (Figure 5).

The relative orientation of helices in the D24N61 subunit *c* structure at pH 5 (Figure 6, center) differs from that of the protonated form of wild-type subunit *c* (Figure 6, left). In the wild-type structure (1A91 and 1C0V), Ala24 is located in the area of closest contact between the two helices. In the latest structure refinement [1C0V (*46*)], the *β*-methyl group

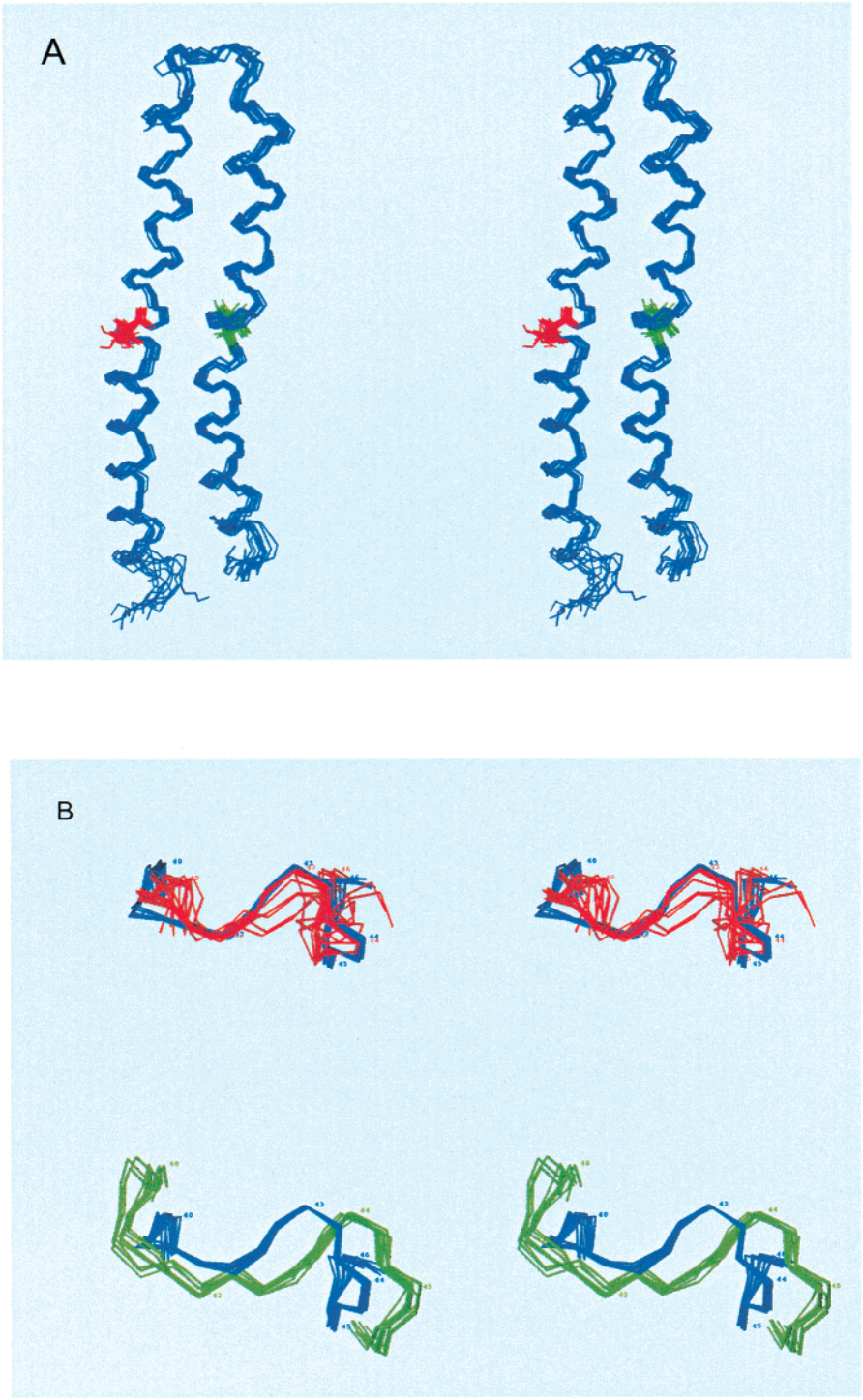

FIGURE 4: Ensemble of the 10 lowest-energy structures of D24N61 subunit *c*. Backbone trace with side chains of Asp24 (red) and Asn61 (green) shown. Polar loop of D24N61 subunit *c* (blue) superimposed on the polar loops of the pH 5 form (1C0V, green) and the pH 8 form (1C99, red) of wild-type subunit *c*.

of Ala24 appears to pack between helices and could be in van der Waals contact with Gly58 and Asp61 on helix 2. Introduction of the bulkier aspartate side chain in this area would require structural rearrangement to avoid steric clashes. In the D24N61 structure, the side chain of Asp24 is located on the front surface of helix 1. This location of Asp24 is brought about largely by a different orientation of the two helices relative to each other such that helix 1 is rotated by 90° clockwise and helix 2 by 150° clockwise relative to their orientation in the wild-type structure (Figure 6B). The helices appear to rotate as units with the structure of individual helices affected little compared to the wild-type structure at pH 5. When segments of the backbone structures of the wild-type and D24N61 proteins are compared, an rmsd of 2.12 Å is calculated for Cα atoms of residues 6−39 and an rmsd of 1.36 Å for Cα atoms of residues 47−76.

In the wild-type protein, the Asp61 side chain is surrounded by hydrophobic side chains of residues Ala20, Met57, Pro64, and Met65 (Figure 7A). This hydrophobic environment may account for the unusually high pK_a of Asp61, which when pK_a = 7.1 is ~1.5 units higher than that of the other two Asp residues and the two Glu residues

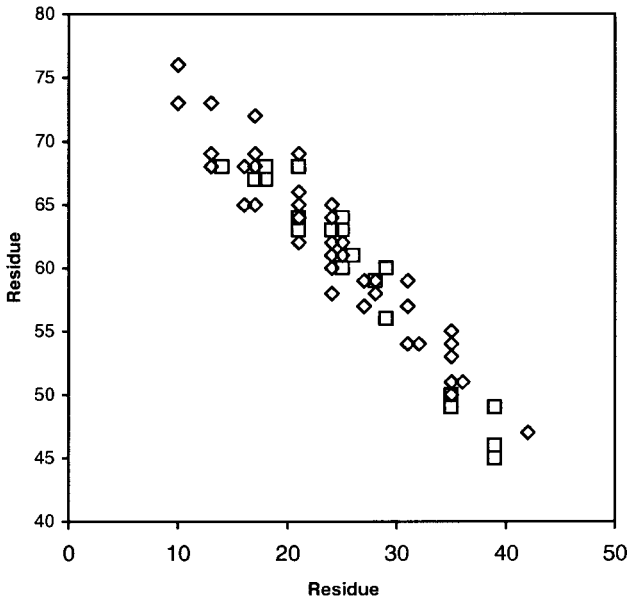

FIGURE 5: Comparison of interhelical NOEs in wild type (◇) and D24N61 substituted (□) subunit *c*.

in the protein (*47*). In D24N61 subunit *c*, Asp24 has a somewhat more exposed position, but the carboxyl group is also flanked by the aliphatic side chains of Ala20, Ala21, Ile28, and Ile63 (Figure 7B). On the other side of the molecule, the Asn61 residue is packed in a cavity created by the aliphatic side chains of Met57 and Met65, with Pro64 and Ala25 packing to one side and Gly58 to the other (Figure 7C). The hydrophobic cavities may explain the elevated pK_as of Asp24 in D24N61 subunit *c* and of both Asp24 and Asp61 in D24D61 subunit *c* (*47*).

The reorientation of helices in the D24N61 mutant protein (Figure 6) has naturally changed the positions of many residues along both helices. Notably, Phe35 and Phe54 at the top and Tyr10, Tyr73, and Phe76 at the bottom of the hairpin are not clustered together as in the wild-type structure at pH 5. Around the proton binding site, Ala62 is found in a more exposed position on the outer surface of helix 2 rather than at the packing interface of the two helices as in the wild type. Gly69, which packs directly at the helix−helix interface in the wild-type protein, is rotated to the outer surface of helix 2.

Further comparison with the wild-type protein reveals that the orientation of the helices (Figure 6) and the conformation of the polar loop (Figure 4B) in the D24N61 structure share greater similarity with the wild-type structure at pH 8, where Asp61 is deprotonated, than to the form at pH 5, where Asp61 is protonated. Indeed, the ensemble rmsds for the backbone atoms of the polar loop (residues 40−46) were 2.4 and 0.6 Å, respectively, when the D24N61 structure was aligned with the low- and high-pH forms of the wild-type protein. Clearly, the conformation of the polar loop in the D24N61 protein is very similar to that of the high-pH form of wild-type subunit *c*.

DISCUSSION

Wild-type subunit *c* is thought to fold in the native F_o complex with Asp61 of TMH-2 close to Ala24 and Ile28 of TMH-1. The genetic evidence for such a juxtaposition includes DCCD-resistant mutants with A24S, I28V, and I28T substitutions in which Asp61 reacts more slowly with DCCD (*72*), inactive mutants with P64I or P64A substitutions that can be suppressed by the second site substitution of A20P with partial or complete restoration of function (*71*, *73*), and carboxyl-interchange substitutions, including A24D/D61G (*49*), A24D/D61S, A24D/D61N (*50*), and, most recently, I28E/D61G or I28D/D61G (*74*), that exhibit significant activity. In addition, Dimroth and co-workers have presented strong evidence that the Na^+ binding site in *Propionigenium modestum* ATP synthase is formed between Gln32, Glu65, and Ser66 (*75*), which correspond to *E. coli* residues 28, 61, and 62, respectively. In the case of *E. coli*, substitution of residues V60, D61, A62, and I63 with A60, E61, S62, and G-, A-, or T63, respectively, led to competitive Li^+ and H^+ binding at Glu61 (*76*). In the initial NMR structure of wild-type subunit *c* at pH 5, the protein was shown to pack in an elongated hairpin of two helices with residues 24 and 28 in TMH-1 close to Asp61 in TMH-2. In cross section, the two helices formed a flattened, ellipsoid-like structure with the side chain of Asp61 packed at the front face and the side chains of Ala24, Ile28, and Ala62 pointing to the back face.[3] To accommodate the predicted residue−residue interactions described above, the subunits were predicted to pack in a "front-to-back" manner in the oligomeric structure, with the ion or inhibitor binding sites formed between two subunits. The prediction of a front-to-back packing was subsequently supported by an extensive cross-linking analysis of Cys-substituted proteins (*22*), by molecular modeling of the *c* oligomeric ring (*24*, *46*), and, most recently, by the fit of the NMR structure to a 3.9 Å resolution electron density map of a mitochondrial F_1−*c* oligomer complex (*32*).

The oligomeric ring model suggested above did not readily accommodate two observations. First, one face of *c*TMH-2, spanning 19 amino acid residues, was shown to cross-link with a 19-residue span of *a*TMH-4 (*35*), but in the oligomeric model, this face of *c*TMH-2 was facing *c*TMH-1 rather than the perimeter of the ring (*24*). Second, Asp61 was predicted to become alternately accessible to entrance and exit channels for H^+ from the two sides of the membrane and also to interact with the essential *a*R210 residue during the proton transport cycle (*20*, *35*, *77*). In the model of the oligomeric ring, the Asp61 side chain was packed at the very center of the four-helix bundle formed by the packing of two *c* subunits in a front-to-back manner. The more recently determined NMR structure of Rastogi and Girvin (*46*), determined at pH 8 where Asp61 is deprotonated, provided a possible structural explanation for the above and suggested a novel mechanism for *c* ring rotation. The packing of the two helices in the pH 8 structure differed from that in the pH 5 structure in that *c*TMH-2 was rotated by 140° relative to *c*TMH-1. Such a rotation would make Asp61 accessible from the periphery of the ring and also make the cross-linkable face of *c*TMH-2 accessible to *a*TMH-4. Rastogi and Girvin (*46*) proposed that, during its transient interaction with subunit *a*, *c*TMH-2 would rotate as Asp61 underwent deprotonation and reprotonation and that the rotation would drive a stepwise movement of the *c* ring. We have considered rotation of *c*TMH-2 as a possible explanation for the cross-linking (*35*) and as the possible driving force for movement of the *c* ring

[3] In a more recent analysis of the data (1C0V), the Ala24 β-methyl group is now positioned more at the interface between helices.

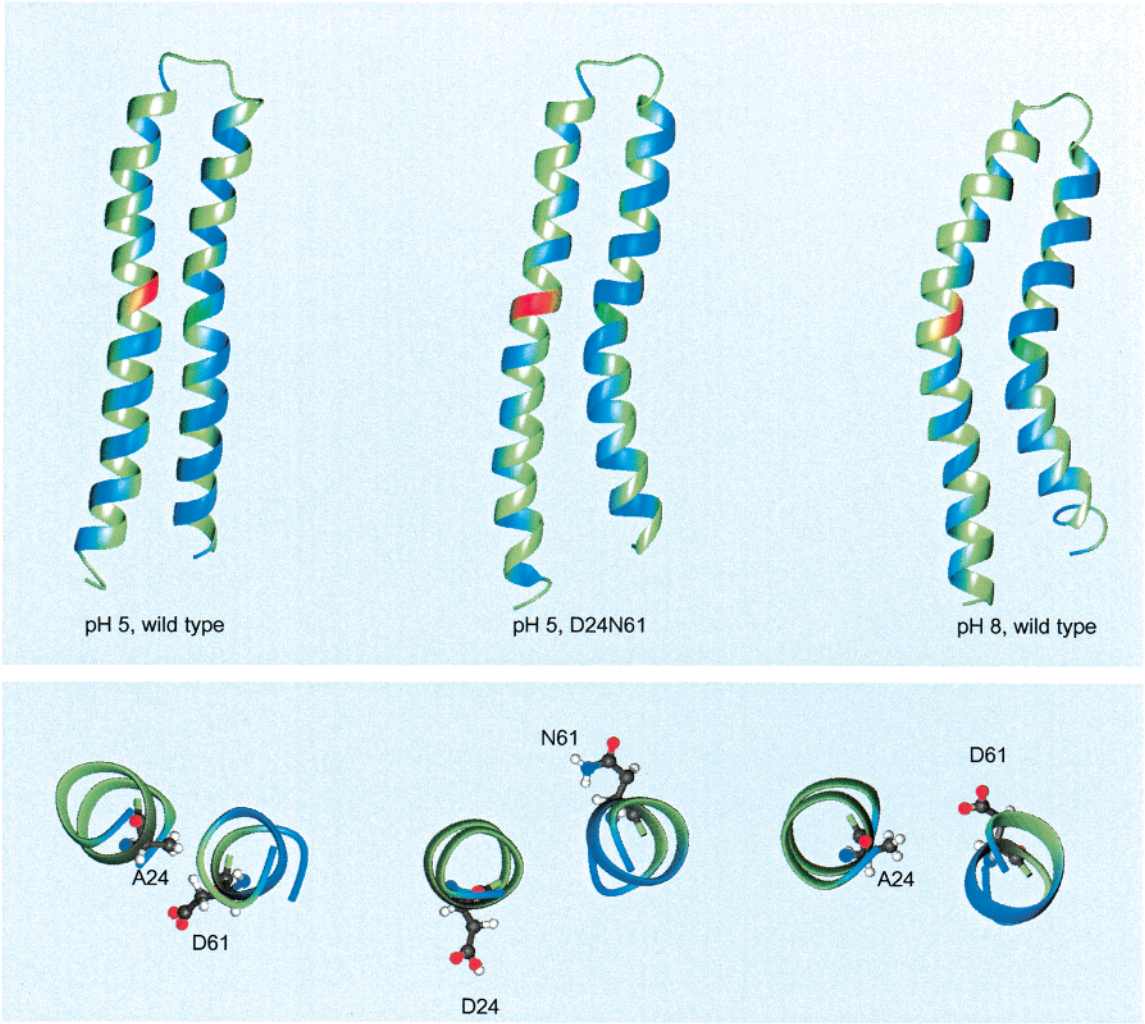

FIGURE 6: Ribbon diagram of the structures of D24N61 subunit *c* (center) and pH 5 (left) and pH 8 (right) forms of wild-type subunit *c*. The backbone segment of every fourth residue beginning with Glu2 is colored blue to show the relative orientation of helices. The position of residue 24 is shown in red. The bottom panel shows the positions of the side chains of residues 24 and 61 as viewed from the polar loop. The Asp61 side chain extends from the front face of the pH 5 wild-type structure.

(*48*). As an alternative, we also considered the possibility that *a*TMH-4 may need to insert between units of the *c* oligomer during the protonation−deprotonation step (*35*, *77*), in part because the helix rotation hypothesis falls short in explaining the function of the *c*TMH-1/TMH-2 carboxyl-interchange mutants (*2*). The structure of the D24N61 carboxyl-interchange mutant described in this paper provides new insights into the possible mechanism and supports a more unifying mechanistic hypothesis.

The NMR structure of the monomeric D24N61 protein and the previous model for the wild-type oligomeric ring were used as the basis for modeling the oligomeric structure for the D24N61 *c* ring. The structure is composed of 10 rather than 12 *c* monomers, but this does not significantly affect the final packing of subunits (*2*, *4*). In the modeling, we have sought the best fit of paired helical segments of the D24N61 monomeric structure to the equivalent helices in the wild-type *c* ring (see Experimental Procedures). The best fit was achieved by aligning helices of a single D24N61 monomer with the helices of two adjacent wild-type monomers as shown in Figure 8. The alignment produced a somewhat different orientation of individual D24N61 subunits in the ring (Figure 8A,B), which is not surprising, since the helices in the mutant protein are rotated around their axes relative to the wild-type structure. In the superposition of the two structures, however, the essential aspartate is located in an equivalent cavity between TMH-1 of one monomer and TMH-2 of its neighbor (Figure 8C). Because TMH-2 of the D24N61 structure is rotated relative to the wild-type structure, the interacting faces of TMH-1 and TMH-2 of two adjacent *c* monomers are nearly the same as in the wild-type oligomer. For example, in both the wild-type and D24N61 models, residue 61 in TMH-2 of one subunit is juxtaposed with residues 28 and 24 in TMH-1 of the next. Moreover, although the model of the D24N61 subunit *c* oligomer has not been tested by Cys−Cys cross-linking, which proved to be so informative in the case of the wild type (*24*), most of the distance constraints used for modeling the wild-type oligomer are satisfied in the model of the D24N61 complex. This includes all TMH-1/TMH-1 and TMH-1/TMH-2 constraints.

What mechanistic insights are suggested by the D24N61 structure? First, the structure provides evidence for two conformational states of the *c* subunit with different relative orientations of the two transmembrane helices. These are exemplified by the pH 5 structure of the wild-type protein on one hand and the structures of the D24N61 protein at pH 5 and wild-type protein at pH 8 on the other. We, therefore,

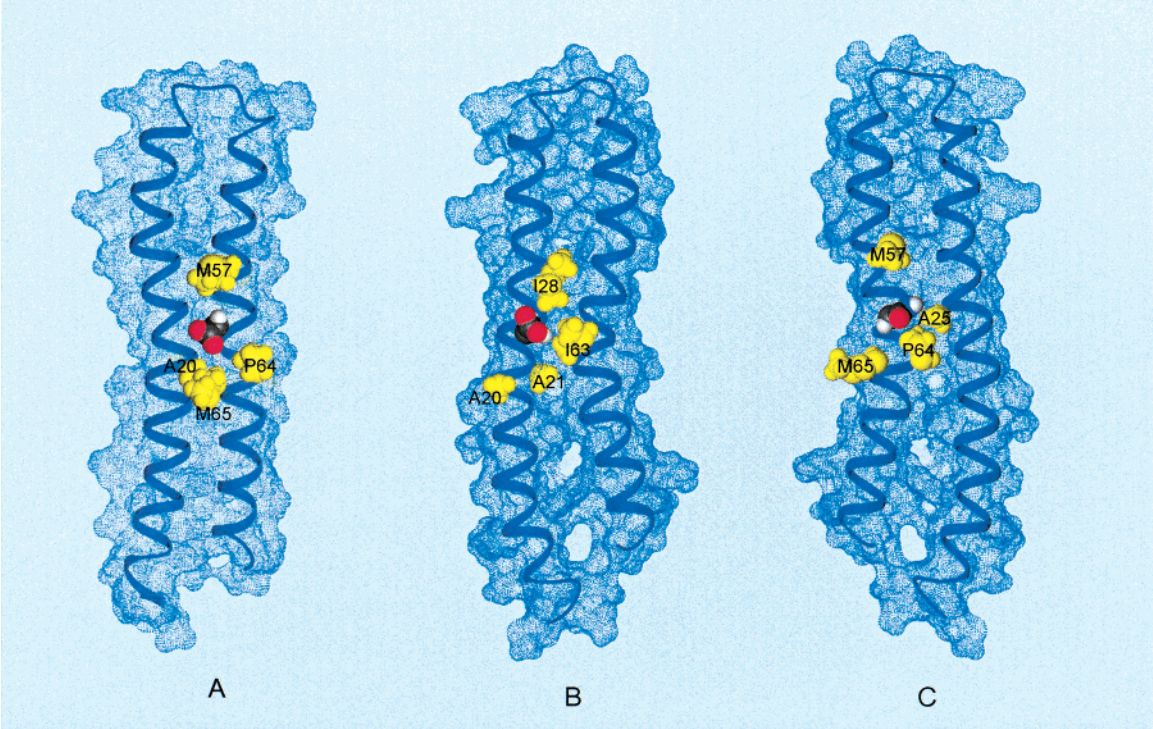

FIGURE 7: Comparison of residues surrounding Asp61 in wild-type subunit *c* at pH 5 to those surrounding Asp24 and Asn61 in D24N61 substituted subunit *c*. (A) Front view of wild-type subunit *c*. (B) Front view of D24N61 subunit *c*. (C) Back view of D24N61 subunit *c*. Asp and Asn side chains are shown in CPK color.

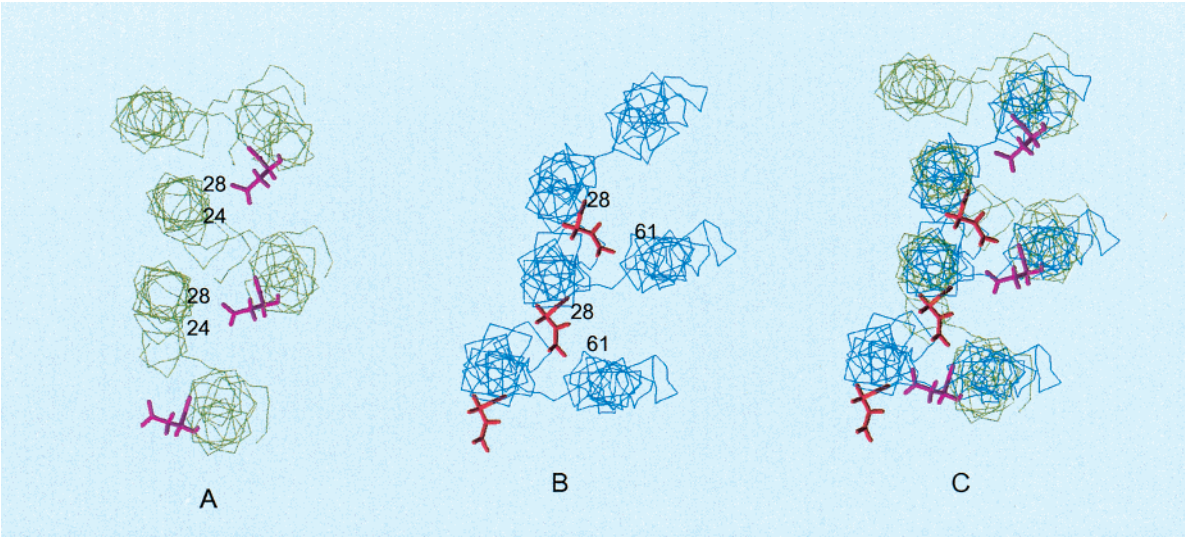

FIGURE 8: Comparison of the proposed oligomeric structures of the *c* ring for wild-type and D24N61 subunit *c*. (A) Proposed oligomeric structure of the wild-type *c* ring based upon NMR structure and cross-linking distance constraints (*24*). Three subunits from a decameric ring are shown with TMH-1 on the inside and TMH-2 on the outside. The side chains of Asp61 and the α-carbon positions for residues Ala24 and Ile28 are also indicated. (B) Best fit model of the D24N61 *c* ring with positioning of the D24N61 subunit onto the wild-type *c* ring carried out as described in the text, again showing three subunits of the decameric ring. The side chains of Asp24 and the α-carbon positions for residues Ile28 and Asn61 are also indicated. (C) Best fit overlay of α-helices of D24N61 subunit *c* on equivalent α-helices of the wild-type ring model. The positions of the Asp24 and Asp61 side chains are indicated.

think that TMH-2 is likely to swivel at some point during the reaction cycle and that the swiveling of the helix will in some way drive rotation of the *c* rotor in agreement with the model of Rastogi and Girvin (*46*; Figure 9A). The pH 5 structure of the D24N61 protein with D24 protonated is more similar to the structure of the deprotonated wild-type protein at pH 8 than it is to the protonated wild-type structure at pH 5. This leads us to question whether rotation of TMH-2 in the *c* oligomer is a direct result of ionization of the essential carboxyl group, as suggested by Rastogi and Girvin (*46*), and to propose that the sequence of events may be more complicated. Second, the modeled structure of the D24N61 oligomer with Asp24 anchored to the inner ring of helices precludes the possibility that the essential carboxyl group leaves its location at the center of the four-helix bundle during TMH-2 rotation. Rastogi and Girvin propose that the essential carboxyl group moves to the periphery of the *c* ring as TMH-2 rotates.

On the basis of these considerations, an adaptation of the Rastogi and Girvin (*46*) model for the wild-type *c* rotor is

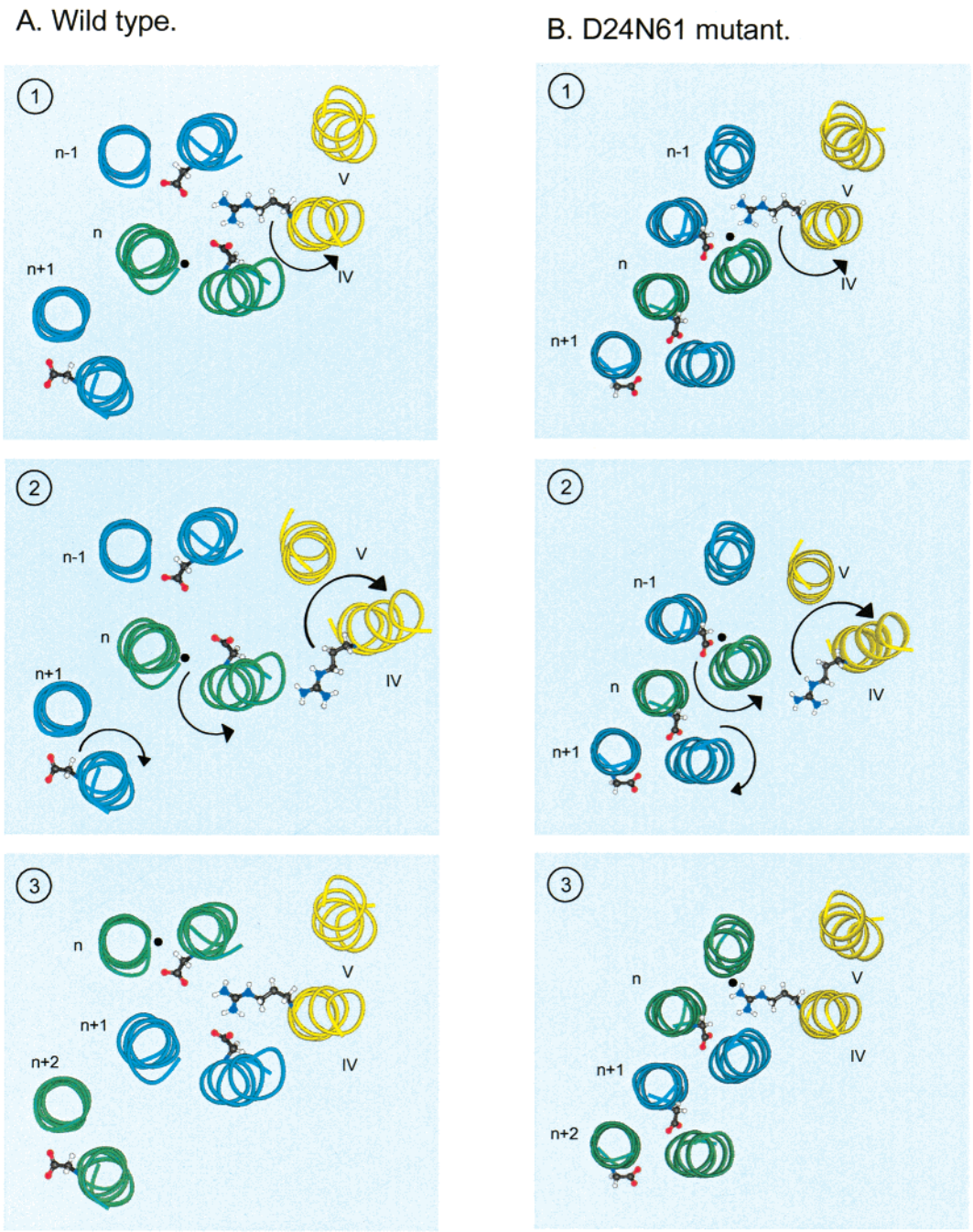

FIGURE 9: Possible adaptation of the rotational model of Rastogi and Girvin (*46*) to the function of D24N61 substituted subunit *c*. (A) Adaptation of the model proposed by Rastogi and Girvin for the wild-type *c* oligomer. In panel 1, a single subunit *c* with Asp61 ionized (the *n*th subunit) is placed in a ring of otherwise protonated subunit *c*. TMH-2 of ionized subunit *c* is rotated relative to TMH-2 of other subunits, with the position of the Asp61 side chain displaced from one side to the other, as in the pH 8 structure. The position of Ala24 of the *n*th subunit is denoted by the black dot. The proposed interaction of ionized Asp61 with *a*Arg210 is indicated. The hypothetical TMH-4 and TMH-5 of subunit *a* are indicated by Roman numerals IV and V, respectively. Following ionization of Asp61, the *a*Arg210 residue is proposed to move away from the ionized Asp61 side chain by a swiveling of *a*TMH4 (shown by the arrow) to generate the structure shown in panel 2. In panel 2, following reprotonation of Asp61, *c*TMH-2 of subunit *n* would rotate back to its original position, as in the pH 5 structure. This rotation would be coupled to the rotation of *a*TMH-4 to reposition *a*Arg210 between subunits *n* and $n + 1$. *c*TMH-2 of subunit $n + 1$ would also rotate to the position indicated in panel 3. These helical movements, indicated by the arrows, would drive the counterclockwise movement of the entire *c* ring. In panel 3 are shown the positions of TMHs and the *c* rotor following movements indicated in panel 2. (B) Adaptation of the Rastogi and Girvin mechanistic model to the modeled ring structure of D24N61 subunit *c*. In panel 1, all three subunits are in the conformation seen in the D24N61 NMR structure. The position of Asn61 in subunit *n* is denoted by the black dot. The *a*Arg210 residue inserted between subunits *n* and $n - 1$ has promoted deprotonation of Asp24 of subunit $n - 1$. In the next step, *a*Arg210 will move away from Asp24_{n-1} by rotation of *a*TMH-4 (see the arrow). In panel 2, following reprotonation of Asp24_{n-1}, helices $c\text{TMH-2}_n$ and *a*TMH-4 rotate in unison and in opposite directions (see arrows) to enable insertion of *a*Arg210 between subunits *n* and $n + 1$ as the rotor is translocated by one step. In panel 3 are shown the final positions following rotor translocation.

shown in Figure 9A. One of the subunits of the oligomeric ring (the *n*th) is shown as in the pH 8 structure with TMH-2 rotated with respect to the other subunits (panel 1 of Figure 9A). The helical rotation leading to this state exposes *c*Asp61 to Arg210 in *a*TMH-4. We think the helical rotation leading to this state of the *n*th subunit is most likely a clockwise

swiveling of the protonated *c*TMH-2, and that Asp61 subsequently deprotonates in the new environment due to its proximity to *a*R210. This sequence would fit best with the structure of the D24N61 protein, determined here, where TMH-2 is turned and Asp24 still protonated. Following deprotonation of Asp61, helical interactions elsewhere in the putative proton channels of subunit *a*, which would be driven by the force of the proton gradient, would cause *a*Arg210 to move from the vicinity of *c*Asp61 to enable reprotonation of the carboxylate group from the periplasmic inlet channel. The position of the *a*Arg210 residue following movement is shown in panel 2 (Figure 9A). Following reprotonation, *c*TMH-2 would then rotate back to its original position with respect to *c*TMH-1 by swiveling in the counterclockwise direction, as shown by the arrow (panel 2 of Figure 9A). This helical rotation would be coupled to the counterclockwise movement of the oligomeric ring, i.e., movement of subunit n to the position occupied by subunit $n - 1$, etc., with the simultaneous swiveling of *c*TMH-2$_{n+1}$ and insertion of *a*R210 between subunits $n + 1$ and n (the final positions are shown in panel 3 of Figure 9A). The latter could occur if the helices of subunits *a* and *c* rotated around each other in a manner akin to meshed gears.

Application of the model to the D24N61 mutant is considered in Figure 9B. In this case, all subunits are shown as resolved in the single NMR structure. The structure of D24N61 subunit at position n resembles wild-type subunit n with Asn61 in TMH-2 positioned proximally to *a*R210 (panel 1 of Figure 9B), i.e., at the same position as is Asp61 in the wild-type model. The insertion of *a*R210 between subunits n and $n - 1$ would in this case lead to the deprotonation of Asp24 of subunit $n - 1$. Following movement of *a*R210, and reprotonation of Asp24$_{n-1}$ from the periplasmic inlet channel (panel 2), TMH-2 of subunit n would then swivel in the counterclockwise direction with *a*TMH-4 rotating in the opposite direction to facilitate movement of the rotor (see the arrows in panel 2 of Figure 9B). These movements would mimic those taking place in the wild-type rotor. The final positions with *a*Arg210 inserted between subunits n and $n + 1$ are shown in panel 3 (Figure 9B). The model as shown leaves open the question of whether TMH-1 also swivels in a concerted fashion during the rotations of TMH-2. Movement of the essential carboxyl from one face of the *c* monomer to the other may be a necessary feature of the ion binding and release interactions at the *a*−*c* interface. A concerted swiveling of both helices would provide a general mechanism that could be applied to either the D24N61 or the wild-type protein.

In summary, the NMR structure of D24N61 subunit *c* leads to a revised view of how conformational changes linked to deprotonation and reprotonation of subunit *c* may drive movement of the *c* rotor. Importantly, the new model seems to be applicable to either wild-type or D24N61 subunit *c*. Previous models required movement of *c*Asp61 to the periphery of the ring during rotation of *c*TMH-2 and did not provide an explanation for the function of the D24N61 mutant (*2*, *46*, *48*). Here, the exposure of the essential aspartate to *a*Arg210 is envisioned as being due to a swiveling of helices and insertion of *a*Arg210 between subunits of the rotor. On the basis of the NMR structure, we make the prediction that *c*TMH-2 swivels before the aspartate is deprotonated and that this movement is a prerequisite for *a*Arg210 subsequently lowering the pK_a of the essential carboxyl group. The movements obviously have to be coupled to the opening and closing of outlet and inlet channels in the still unresolved structure of subunit *a*. We believe that many of the predictions of this model can be tested by biochemical methods that are now at hand.

ACKNOWLEDGMENT

This paper is dedicated to Professor Karlheinz Altendorf on his 60th birthday. Herzlichen Glückwunsch, Karlheinz!

REFERENCES

1. Senior, A. E. (1988) *Physiol. Rev. 68*, 177−231.
2. Fillingame, R. H., Jiang, W., and Dmitriev, O. Y. (2000) *J. Bioenerg. Biomembr. 32*, 433−439.
3. Foster, D. L., and Fillingame, R. H. (1982) *J. Biol. Chem. 257*, 2009−2015.
4. Jiang, W., Hermolin, J., and Fillingame, R. H. (2001) *Proc. Natl. Acad. Sci. U.S.A. 98*, 4966−4971.
5. Abrahams, J. P., Leslie, A. G. W., Lutter, R., and Walker, J. E. (1994) *Nature 370*, 621−628.
6. Duncan, T. M., Bulygin, V. V., Zhou, Y., Hutcheon, M. L., and Cross, R. L. (1995) *Proc. Natl. Acad. Sci. U.S.A. 92*, 10964−10968.
7. Sabbert, D., Engelbrecht, S., and Junge, W. (1996) *Nature 381*, 623−625.
8. Noji, H., Yasuda, R., Yoshida, M., and Kinosita, K., Jr. (1997) *Nature 386*, 299−302.
9. Weber, J., and Senior, A. E. (2000) *Biochim. Biophys. Acta 1458*, 300−309.
10. Tang, C., and Capaldi, R. A. (1996) *J. Biol. Chem. 271*, 3018−3024.
11. Kato-Yamada, Y., Noji, H., Yasuda, R., Kinosita, K., Jr., and Yoshida, M. (1998) *J. Biol. Chem. 273*, 19375−19377.
12. Rodgers, A. J. W., and Wilce, M. C. J. (2000) *Nat. Struct. Biol. 7*, 1051−1054.
13. Gibbons, C., Montgomery, M. G., Leslie, A. G. W., and Walker, J. E. (2000) *Nat. Struct. Biol. 7*, 1055−1061.
14. Sambongi, Y., Iko, Y., Tanabe, M., Omote, H., Iwamoto-Kihara, A., Ueda, I., Yanagida, T., Wada, Y., and Futai, M. (1999) *Science 286*, 1722−1724.
15. Pänke, O., Gumbiowski, K., Junge, W., and Engelbrecht, S. (2000) *FEBS Lett. 472*, 34−38.
16. Tanabe, M., Nishio, K., Iko, Y., Sambongi, Y., Iwamoto-Kihara, A., Wada, Y., and Futai, M. (2001) *J. Biol. Chem. 276*, 15269−15274.
17. Tsunoda, S. P., Aggeler, R., Yoshida, M., and Capaldi, R. A. (2001) *Proc. Natl. Acad. Sci. U.S.A. 98*, 898−902.
18. Vik, S. B., and Antonio, B. J. (1994) *J. Biol. Chem. 269*, 30364−30369.
19. Engelbrecht, S., and Junge, W. (1997) *FEBS Lett. 414*, 485−491.
20. Elston, T., Wang, H., and Oster, G. (1998) *Nature 391*, 510−513.
21. Girvin, M. E., Rastogi, V. K., Abildgaard, F., Markley, J. L., and Fillingame, R. H. (1998) *Biochemistry 37*, 8817−8824.
22. Jones, P. C., Jiang, W., and Fillingame, R. H. (1998) *J. Biol. Chem. 273*, 17178−17185.
23. Jones, P. C., and Fillingame, R. H. (1998) *J. Biol. Chem. 273*, 29701−29705.
24. Dmitriev, O. Y., Jones, P. C., and Fillingame, R. H. (1999) *Proc. Natl. Acad. Sci. U.S.A. 96*, 7785−7790.
25. Zhang, Y., and Fillingame, R. H. (1995) *J. Biol. Chem. 270*, 24609−24614.
26. Watts, S. D., Teng, C., and Capaldi, R. A. (1996) *J. Biol. Chem. 271*, 28314−28347.
27. Wilkens, S., Dahlquist, F. W., McIntosh, L. P., Donaldson, L. W., and Capaldi, R. A. (1995) *Nat. Struct. Biol. 2*, 961−967.
28. Hermolin, J., Dmitriev, O. Y., Zhang, Y., and Fillingame, R. H. (1999) *J. Biol. Chem. 274*, 17011−17016.

29. Birkenhäger, R., Hoppert, M., Deckers-Hebestreit, G., Mayer, F., and Altendorf, K. (1995) *Eur. J. Biochem. 230*, 58−67.
30. Takeyasu, K., Omote, H., Nettikadan, S., Tokumasu, F., Iwamoto-Kihara, A., and Futai, M. (1996) *FEBS Lett. 392*, 110−113.
31. Singh, S., Turina, P., Bustamante, C. J., Keller, D. J., and Capaldi, R. A. (1996) *FEBS Lett. 397*, 30−34.
32. Stock, D., Leslie, A. G. W., and Walker, J. E. (1999) *Science 286*, 1700−1705.
33. Seelert, H., Poetsch, A., Dencher, N. A., Engel, A., Stahlberg, H., and Müller, D. J. (2000) *Nature 405*, 418−419.
34. Stahlberg, H., Müller, D. J., Suda, K., Fotiadis, D., Engel, A., Meier, T., Matthey, U., and Dimroth, P. (2001) *EMBO Rep. 2*, 229−233.
35. Jiang, W., and Fillingame, R. H. (1998) *Proc. Natl. Acad. Sci. U.S.A. 95*, 6607−6612.
36. Dunn, S. D., McLachlin, D. T., and Revington, M. (2000) *Biochim. Biophys. Acta 1458*, 356−363.
37. Capaldi, R. A., Schulenberg, B., Murray, J., and Aggeler, R. (2000) *J. Exp. Biol. 203*, 29−33.
38. Altendorf, K., Stalz, W.-D., Greie, J.-C., and Deckers-Hebestreit, G. (2000) *J. Exp. Biol. 203*, 19−28.
39. Dmitriev, O., Jones, P. C., Jiang, W., and Fillingame, R. H. (1999) *J. Biol. Chem. 274*, 15598−15604.
40. Jones, P. J., Hermolin, J., Jiang, W., and Fillingame, R. H. (2000) *J. Biol. Chem. 275*, 31340−31346.
41. Rodgers, A. J. W., and Capaldi, R. A. (1998) *J. Biol. Chem. 273*, 29406−29410.
42. McLachlin, D. T., and Dunn, S. D. (2000) *Biochemistry 39*, 3486−3490.
43. Valiyaveetil, F. I., and Fillingame, R. H. (1998) *J. Biol. Chem. 273*, 16241−16247.
44. Wada, T., Long, J. C., Zhang, D., and Vik, S. B. (1999) *J. Biol. Chem. 274*, 17353−17357.
45. Fraga, D., Hermolin, J., and Fillingame, R. H. (1994) *J. Biol. Chem. 269*, 2562−2567.
46. Rastogi, V. K., and Girvin, M. E. (1999) *Nature 402*, 263−268.
47. Assadi-Porter, F. M., and Fillingame, R. H. (1995) *Biochemistry 34*, 16186−16193.
48. Fillingame, R. H., Jiang, W., and Dmitriev, O. Y. (2000) *J. Exp. Biol. 203*, 9−17.
49. Miller, M. J., Oldenburg, M., and Fillingame, R. H. (1990) *Proc. Natl. Acad. Sci. U.S.A. 87*, 4900−4904.
50. Zhang, Y., and Fillingame, R. H. (1994) *J. Biol. Chem. 269*, 5473−5479.
51. Fraga, D., Hermolin, J., and Fillingame, R. H. (1994) *J. Biol. Chem. 269*, 2562−2567.
52. Girvin, M. E., and Fillingame, R. H. (1993) *Biochemistry 32*, 12167−12177.
53. Mori, S., Abeygunawardana, C., Johnson, M. O., and van Zijl, P. C. (1995) *J. Magn. Reson., Ser. B 108*, 94−98.
54. Kay, L. E., Xu, G. Y., and Yamazaki, T. (1994) *J. Magn. Reson., Ser. A 101*, 129−133.
55. Yamazaki, T., Lee, W., Revington, M., Mattiello, D. L., Dahlquist, F. W., Arrowsmith, C. H., and Kay, L. E. (1994) *J. Am. Chem. Soc. 116*, 6464−6465.
56. Grzesiek, S., and Bax, A. (1992) *J. Am. Chem. Soc. 114*, 6291−6293.
57. Powers, R., Gronenborn, A. M., Clore, G. M., and Bax, A. (1991) *J. Magn. Reson. 94*, 209.
58. Yamazaki, T., Lee, W., Arrowsmith, C. H., Muhandiram, D. R., and Kay, L. E. (1994) *J. Am. Chem. Soc. 116*, 11655−11666.
59. Kay, L. E., Xu, G. Y., Singer, A. U., Muhandiram, R., and Forman-Kay, J. D. (1993) *J. Magn. Reson., Ser. B 101*, 333−337.
60. Grzesiek, S., Anglister, J., and Bax, A. (1993) *J. Magn. Reson., Ser. B 101*, 114−119.
61. Talluri, S., and Wagner, G. (1996) *J. Magn. Reson., Ser. B 112*, 200−205.
62. Zhang, O., Kay, L. E., Olivier, J. P., and Forman-Kay, J. D. (1994) *J. Biomol. NMR 6*, 845−858.
63. Zhang, W., Smithgall, T. E., and Gmeiner, W. H. (1996) *J. Magn. Reson., Ser. B 111*, 305−309.
64. Muhandiram, R., Xu, G. Y., and Kay, L. E. (1993) *J. Biomol. NMR 3*, 463−470.
65. Vuister, G. W., Clore, G. M., Gronenborn, A. M., Powers, R., and Garrett, D. S. (1993) *J. Magn. Reson., Ser. B 101*, 210−213.
66. Chylla, R. A., Volkman, B. F., and Markley, J. L. (1998) *J. Biomol. NMR 12*, 277−297.
67. Güntert, P., Mumenthaler, C., and Wüthrich, K. (1997*) J. Mol. Biol. 273*, 283−298.
68. Laskowski, R. A., MacArthur, M. W., Moss, D. S., and Thornton, J. M. (1993) *J. Appl. Crystallogr. 26*, 283−291.
69. Koradi, R., Billeter, M., and Wüthrich, K. (1996) *J. Mol. Graphics 14*, 51−55.
70. Brunger, A. T., Adams, P. D., Clore, G. M., Delano, W. L., Gros, P., Grosse-Kunstleve, R. W., Jiang, J.-S., Kuszewski, J., Nilges, N., Pannu, N. S., Read, R. J., Rice, L. M., Simonson, T., and Warren, G. L. (1998) *Acta Crystallogr. D54*, 905−921.
71. Dmitriev, O. Y., and Fillingame, R. H. (2001) *J. Biol. Chem. 276*, 27449−27454.
72. Fillingame, R. H., Oldenburg, M., and Fraga, D. (1991) *J. Biol. Chem. 266*, 20934−20939.
73. Fimmel, A. L., Jans, D. A., Langman, L., James, L. B., Ash, G. R., Downie, J. A., Senior, A. E., Gibson, F., and Cox, G. B. (1983) *Biochem. J. 213*, 451−458.
74. Jones, P. C. (2001) *J. Bacteriol. 183*, 1524−1530.
75. Kaim, G., Wehrle, F., Gerike, U., and Dimroth, P. (1997) *Biochemistry 36*, 9185−9194.
76. Zhang, Y., and Fillingame, R. H. (1995) *J. Biol. Chem. 270*, 87−93.
77. Fillingame, R. H., Jiang, W., Dmitriev, O. Y., and Jones, P. C. (2000) *Biochim. Biophys. Acta 1458*, 387−403.

BI012198L